Finite-thickness effects on the Rayleigh-Taylor instability in accelerated elastic solids

S. A. Piriz and A. R. Piriz*
Instituto de Investigaciones Energéticas, ETSII, and CYTEMA, Universidad de Castilla-La Mancha, 13071 Ciudad Real, Spain

N. A. Tahir
GSI Helmholtzzentrum für Schwerionenforschung Darmstadt, Planckstrasse 1, 64291 Darmstadt, Germany
(Received 18 February 2017; revised manuscript received 14 April 2017; published 17 May 2017)

A physical model has been developed for the linear Rayleigh-Taylor instability of a finite-thickness elastic slab laying on top of a semi-infinite ideal fluid. The model includes the nonideal effects of elasticity as boundary conditions at the top and bottom interfaces of the slab and also takes into account the finite transit time of the elastic waves across the slab thickness. For Atwood number $A_T = 1$, the asymptotic growth rate is found to be in excellent agreement with the exact solution [Plohr and Sharp, Z. Angew. Math. Mech. **49**, 786 (1998)], and a physical explanation is given for the reduction of the stabilizing effectiveness of the elasticity for the thinner slabs. The feedthrough factor is also calculated.

DOI: 10.1103/PhysRevE.95.053108

I. INTRODUCTION

Rayleigh-Taylor instability (RTI) in accelerated solids that retain their mechanical properties during the acceleration process is of great importance in many physical situations involving high energy density (HED) matter [1–28]. In particular, it is of relevance for the Laboratory of Planetary Sciences (LAPLAS) experimental set, which will be a central piece of the research program on HED physics to be developed at the Facility for Antiproton and Ion Research (FAIR), now under construction at the GSI Helmholtzzentrum für Schwerionenforschung in Darmstadt, Germany [11–22].

LAPLAS will be mainly directed to study the thermophysical properties of matter under extreme conditions such as the ones that could be found in the core of giant gaseous or Earth-like planets. In these experiments a sample material will be quasi-isentropically compressed by the implosion of a cylindrical heavy metal shell (W or Ta) driven by an intense heavy ion beam with a ring shaped focal spot [21,22,29].

The implosion of cylindrical metallic shells (liners) is also used in experiments in which the acceleration is driven by very intense pulsed electrical currents. These experiments are performed in the framework of the novel magnetic liner inertial fusion (MagLIF) approach to the inertial fusion [23–28]. Although it has some similarities to MagLIF, LAPLAS will work in a rather different regime involving considerably lower aspect ratios and accelerations, as well as a much denser pusher. Therefore, sufficient mitigation or even suppression of RTI is expected in LAPLAS to be provided by the mechanical strength of the heavy metal shell.

In addition, RTI in accelerated slabs has become a current method to test physical models for the constitutive properties of matter under very high strain and strain rate conditions. To this end, experiments with planar slabs accelerated by explosives or by laser ablation have been performed to evaluate yield strength Y and shear modulus G of solids at such extreme conditions [1–10]. More recently, Richtmyer-Meshkov instability has also been used for similar purposes [30–34].

The nonlinear character of the constitutive equations for an elastic-plastic solid has led to the development of approximate physical models that provide a theoretical description of the RTI evolution [3,4,35–48]. Exact theories have been advanced only for the case of RTI in purely elastic (Hookean) solids [49,50], and although they have great relevance for testing the quality of the previously mentioned approximations, they have been found to be too complex to allow a relatively simple extension that could include the transition to the plastic regime. Furthermore, most of these studies have been constrained to an interface between two semi-infinite media, with the only exceptions being the exact theory of Ref. [49] for arbitrary thickness and the model reported in Refs. [3,4] for a very thin layer, both for Atwood number $A_T = 1$.

On the other hand, the problem of the finite-thickness effects on RTI in a slab of ideal fluid with a top free surface was first considered by Taylor [51,52]. These results were later extended by Mikaelian to consider the presence of ideal fluids above and below the slab [53,54] and the effect of the surface tension on both interfaces of the slab [55]. A similar analysis was more recently presented in order to consider the presence of magnetic fields on both sides and inside an ideal fluid slab [56,57]. Some other works were also carried out in the framework of geophysical and biophysical applications in which a slab of viscous fluid with a top free surface was considered. However, these cases were treated by using very rough approximations [58] or limited to the regime of small Reynolds numbers [59–62].

More detailed work was instead presented for the case of a slab of viscous fluid with a top rigid surface [63]. In this case, the presence of such a rigid surface reduces the number of boundary conditions and considerably simplifies the problem, but such a rigid surface boundary condition is not appropriate for dealing with accelerated slabs that are not confined by material surfaces.

In this paper we deal with the problem of RTI in a perfectly elastic solid slab of finite thickness with a top free surface lying on a semi-infinite ideal fluid. The aim is to present an approximate theory for the RTI that may later allow for a relatively simple extension that would include the transition to

*roberto.piriz@uclm.es

the plastic regime, like what was done in the past for RTI in semi-infinite media [35,41,42].

In this regard, the consideration of a medium as semi-infinite is expected to be valid provided that the transit time $t_T \sim h/c_e$ of the elastic waves through the slab thickness (where h is the thickness of the slab, $c_e = \sqrt{G/\rho}$ is the propagation velocity of the elastic waves, and ρ is the slab density) is larger than the characteristic RTI growth time $t_{RT} = \gamma_{\max}^{-1}$ (where $\gamma_{\max}$ is the maximum value of the growth rate γ). By taking $\gamma_{\max} \sim \sqrt{k_0 g}$, with $k_0 = \rho g/G$, the condition $t_T > t_{RT}$ leads to

$$k_0 h > 1, \tag{1}$$

or $p_0 > G$, where $p_0 = \rho g h$ is the pressure driving the slab acceleration. That is, such a condition may not be satisfied in many experiments using high explosives to accelerate a heavy metal slab, and certainly, it will not be fulfilled in the LAPLAS experiments where shells of heavy metal with $G > 100$ to 200 GPa are being considered, and the driving pressures will not be high enough to satisfy Eq. (1), especially in the initial phases of FAIR operation when full intensity will not yet be available.

We have shown in the past that relatively simple physical models can be constructed, with reasonable accuracy, by adding specific issues resulting from some physical insight into the problem. In fact, often, a great deal of mathematical complications stands for only a small part of the physics, and the identification of some significant physical aspect of the problem may bring an important simplification of the mathematical problem, while still capturing the most relevant features. Such simplifications may also allow for the consideration of more complex problems that are difficult to treat by means of exact methods.

Here we will consider the effect of the finite thickness of an elastic medium on RTI by taking into account that, due to the finite transit time of the elastic waves across the slab, the restoring elastic forces that resist deformation caused by the perturbation growth are produced by the total strain of the slab rather than by the local strain.

Moreover, we will assume as in Refs. [35–48] that the velocity field arising from the perturbation evolution of the unstable interface can be well described by the irrotational and solenoidal field and that the elastic effects can be effectively introduced through the boundary conditions at the edges of the elastic slab. Further discussion is presented in Appendix B.

In Sec. II we first review the derivation of the asymptotic growth rate for the RTI in a finite-thickness slab of ideal fluid floating on a less dense semi-infinite ideal fluid. Then, a model is presented for the case in which the slab consists of a perfectly elastic medium. The results of the model are discussed in Sec. III, including the calculation of the feedthrough factor for the transmission of the perturbation from the bottom to the top interface. Some conclusions are summarized in Sec. IV.

II. THE ANALYTICAL MODEL

We consider the simplest case shown in Fig. 1 for a perfectly elastic solid slab of thickness h, density ρ_2, and shear modulus G lying on a semi-infinite ideal fluid of density $\rho_1 < \rho_2$ in a uniform gravitational field $\vec{g} = g\mathbf{e_y}$. For $y \leqslant -h$ we take density $\rho_3 = 0$.

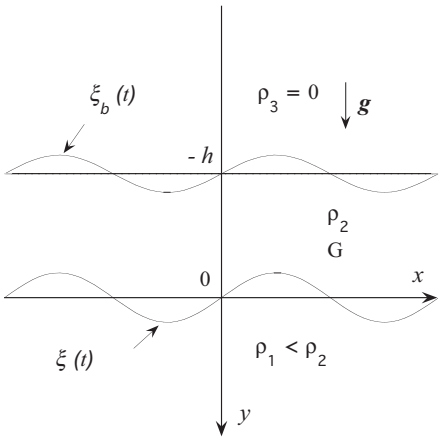

FIG. 1. Schematic of the two-interface system formed by the elastic slab on top of an ideal fluid.

We first briefly review the case in which the slab is also an ideal fluid ($G = 0$) [51,52].

A. Finite-thickness ideal fluid slab ($G = 0$)

In this case the velocity field turns out to be irrotational, and assuming incompressible perturbations, the vertical velocity is obtained (see Appendix A) as

$$\begin{aligned} \delta v_{2y} &= e^{ikx}(A_+ e^{ky} + A_- e^{-ky}), \quad -h \leqslant y \leqslant 0, \\ \delta v_{1y} &= e^{ikx} B_- e^{-ky}, \quad y \geqslant 0, \end{aligned} \tag{2}$$

and pressure perturbations turn out to be

$$\begin{aligned} \delta p_2 &= -\frac{\rho_2}{k} e^{ikx}(\dot{A}_+ e^{ky} - \dot{A}_- e^{-ky}), \quad -h \leqslant y \leqslant 0, \\ \delta p_1 &= \frac{\rho_1}{k} e^{ikx} \dot{B}_- e^{-ky}, \quad \text{for } y \geqslant 0, \end{aligned} \tag{3}$$

where $k = 2\pi/\lambda$ is the perturbation wave number (λ is the perturbation wavelength) and overdots indicate time derivatives. In addition, the boundary conditions at $y = 0$ read

$$A_+ + A_- = \dot{\xi} = B_-, \tag{4}$$

$$\delta p_1(0) - \delta p_2(0) = (\rho_2 - \rho_1) g \xi, \tag{5}$$

where $\xi = \xi(t)$ is the instantaneous maximum perturbation amplitude at $y = 0$ (Fig. 1). In the same manner at $y = -h$, we have

$$A_+ e^{-kh} + A_- e^{hk} = \dot{\xi}_b, \tag{6}$$

$$\delta p_2(-h) = -\rho_2 g \xi_b, \tag{7}$$

where $\xi_b = \xi_b(t)$ is the instantaneous maximum perturbation amplitude at $y = -h$. By considering the asymptotic regime with $\xi \sim \xi_b \sim e^{\gamma t}$, where γ is the instability growth rate, the previous equations yield

$$\frac{\gamma^2 \rho_1}{k} \xi + \frac{\gamma \rho_2}{k}(A_+ - A_-) = (\rho_2 - \rho_1) g \xi, \tag{8}$$

$$A_+ + A_- = \gamma \xi, \tag{9}$$

$$A_+e^{-kh} + A_-e^{hk} = \gamma\xi_b, \tag{10}$$

$$\frac{\gamma\rho_2}{k}(A_+e^{-kh} - A_-e^{kh}) = \rho_2 g\xi_b. \tag{11}$$

The solution of Eqs. (8) to (11) is straightforward, and it reads

$$A_- = A_+ f = \frac{\gamma\xi f}{1+f}, \quad f = \frac{\gamma^2 - kg}{\gamma^2 + kg}e^{-2kh}, \tag{12}$$

and the instability growth rate turns out to be given by the following expression [51,52]:

$$\gamma = \sqrt{\frac{(\rho_2 - \rho_1)kg}{\rho_2 + \rho_1 \coth kh}}. \tag{13}$$

It is easily appreciated that when $kh \to \infty$, the classical growth rate $\sqrt{A_T kg}$ is recovered [where $A_T = (\rho_2 - \rho_1)/(\rho_2 + \rho_1)$]. In addition, it is seen that except for $A_T = 1$ ($\rho_1 = 0$) the growth rate is lower for thinner slabs. This is essentially because the "stable" upper interface presents some resistance to the deformation that is more effective the thinner the slab is.

B. Elastic solid slab on the top of an ideal fluid

We consider now that the slab is a Hookean solid characterized by a shear modulus G as shown in Fig. 1. Following Refs. [35–48], we assume that the effect of the elasticity of the solid slab can be introduced as a boundary condition at the top and bottom edges of the slab. Then Eqs. (5) and (7) are modified by the presence of the forces per unitary surface S_a and S_b at $y = 0$ and $y = -h$, respectively:

$$\delta p_1(0) - \delta p_2(0) = (\rho_2 - \rho_1)g\xi - S_a, \tag{14}$$

$$\delta p_2(-h) = -\rho_2 g\xi_b - S_b. \tag{15}$$

Then, Eqs. (8) and (11) are, respectively, replaced by the following equations when an elastic solid slab is considered:

$$\frac{\gamma^2\rho_1}{k}\xi + \frac{\gamma\rho_2}{k}(A_+ - A_-) = (\rho_2 - \rho_1)g\xi - S_a, \tag{16}$$

$$\frac{\gamma\rho_2}{k}(A_+e^{-kh} - A_-e^{kh}) = \rho_2 g\xi_b + S_b. \tag{17}$$

The forces S_a and S_b are determined by the vertical component S_{yy} of the deviatoric part of the stress tensor (given by Hooke's law), which in the asymptotic regime can be written as follows [35,36,47]:

$$\gamma S_{yy} = 2GD_{yy}, \tag{18}$$

where

$$D_{yy} = \frac{\partial(\delta v_{2y})}{\partial y} = k(A_+e^{+ky} - A_-e^{-ky}). \tag{19}$$

D_{yy} is the component of the strain rate tensor normal to the unperturbed interface, and we have evaluated it by using the irrotational velocity field given by Eqs. (2).

For the case $kh \gg 1$, the previous expressions yield

$$S_a = S_{yy}(y = 0) = 2kG\xi,$$
$$S_b = S_{yy}(y = -h \to -\infty) = 0, \tag{20}$$

and the problem reduces to the one considered in Ref. [35] for a single interface between an elastic medium and an ideal fluid. In the opposite case, when $kh < 1$, the transit time of the elastic waves becomes shorter than the characteristic time of growth of the instability. That is, the elastic forces acting at the edges of the solid slab will not be determined by the local strains occurring near the interfaces and are a consequence of the total strain of the slab. Both extreme cases can be well accounted for by taking $S_a = S_b = S$, where S is the result of the total strain:

$$\gamma S = 2G\int_{-h}^{0} dD_{yy} = 2G[D_{yy}(0) - D_{yy}(-h)]. \tag{21}$$

It is worth noticing that, because of the decaying mode of the velocity field δv_{2y}, the case of a single interface for a semi-infinite elastic medium is retrieved once again for $h \to \infty$. Therefore, Eq. (21) is actually suitable for all values of kh, and we will use it in Eqs. (16) and (17).

Then, from Eq. (17) together with Eqs. (9) and (10) we can get

$$A_- = \frac{\gamma\xi f}{1+f} - \frac{\gamma k e^{-kh}}{\rho_2(1+f)(\gamma^2 + kg)}S, \tag{22}$$

$$A_+ = \frac{\gamma\xi f}{1+f} + \frac{\gamma k e^{-kh}}{\rho_2(1+f)(\gamma^2 + kg)}S, \tag{23}$$

with f defined in Eq. (12). Thus, by introducing Eqs. (22) and (23) into Eq. (16), the following equation for the instability growth rate is obtained in terms of S:

$$\gamma^2(\rho_2 + \rho_1) - (\rho_2 - \rho_1)kg$$
$$= (\gamma^2 + kg)(\rho_2 - \rho_1)f - \frac{kS}{\xi}(1+f)$$
$$\times\left[1 + \frac{2\gamma^2 e^{-kh}}{(1+f)(\gamma^2 + kg)}\right]. \tag{24}$$

It is not difficult to check that when $S = 0$, the previous equation for the growth rate reduces to Eq. (13).

On the other hand, in order to calculate S we adopt a further approximation which produces a simpler expression that is still pretty accurate. It consists of using the expressions given by Eq. (12) for $A_\pm$ in Eq. (19), so that Eq. (21) yields

$$S \approx \frac{2kG\xi}{\gamma^2 + kg}\frac{1 - e^{-2kh}}{1+f}\left(\gamma^2 + kg\tanh\frac{kh}{2}\right), \tag{25}$$

and after some algebra, the instability growth rate reads as follows:

$$\gamma^2(\rho_2 + \rho_1\coth kh) - (\rho_2 - \rho_1)kg$$
$$+ \frac{2k^2G}{\gamma^2 + kg}\left(\gamma^2 + kg\tanh\frac{kh}{2}\right)$$
$$\times\left[1 + \frac{2\gamma^2 e^{-kh}}{(1+f)(\gamma^2 + kg)}\right] = 0. \tag{26}$$

In order to solve this equation it is convenient to introduce the following dimensional magnitudes:

$$\kappa = \frac{k}{k_0}, \quad \sigma = \frac{\gamma}{\sqrt{k_0 g}}, \quad k_0 = \frac{\rho_2 g}{G}. \tag{27}$$

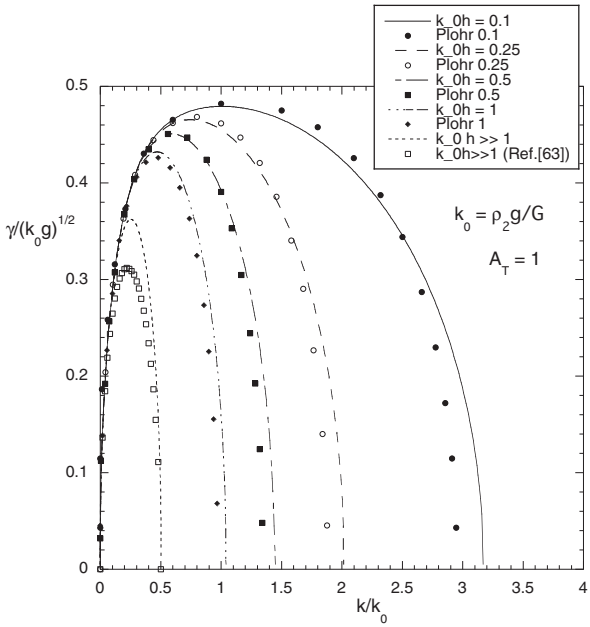

FIG. 2. Asymptotic dimensionless growth rate $\sigma = \gamma/\sqrt{k_0 g}$ as a function of the dimensionless wave number $\kappa = k/k_0$ for several values of $a = k_0 h$ and $A_T = 1$. Dots for $a \leqslant 1$ are calculated with the theory of Ref. [49], and for $a \gg 1$ Ref. [50] has been used.

Then, we have

$$k_0 h = \frac{\rho_2 g h}{G} \equiv a, \quad f = \frac{\sigma^2 - \kappa}{\sigma^2 + \kappa} e^{-2a\kappa}, \tag{28}$$

and the equation for the dimensionless growth rate σ is written as follows:

$$\sigma^2 \left(1 + \frac{1 - A_T}{1 + A_T} \coth a\kappa\right) - \frac{2A_T}{1 + A_T}\kappa + \frac{2\kappa^2}{\sigma^2 + \kappa}\left(\sigma^2 + \kappa \tanh \frac{a\kappa}{2}\right)\frac{\kappa + \sigma^2 \coth(a\kappa/2)}{\kappa + \sigma^2 \coth a\kappa} = 0. \tag{29}$$

III. MODEL RESULTS

A. Instability growth rate

Equation (29) for $\sigma(\kappa)$ is a bicubic polynomial that has a unique real and positive root in the interval $0 \leqslant \kappa \leqslant \kappa_c$, where κ_c is the dimensionless wave number beyond which elasticity completely stabilizes the solid slab. In such an interval we calculate the dimensionless growth rate $\sigma(\kappa)$ and compare it with the results for $A_T = 1$ reported in Ref. [49]. The comparison is shown in Fig. 2 for several values of $a = k_0 h$ (0.1, 0.25, 0.5, 1, and $a \gg 1$). The model reduces to that of Ref. [35] for the case of $a \gg 1$, and as discussed in that work, it has a maximum difference of 18% from the exact results of Refs. [49,50]. For $a \leqslant 1$, the present model is in excellent agreement with the exact results of Ref. [49] and with the approximate model for a very thin slab reported in Refs. [3,4] (both for $A_T = 1$). For $a \leqslant 1$ the maximum discrepancy is in the cutoff wave number κ_c, which differs less than 7% from the exact result.

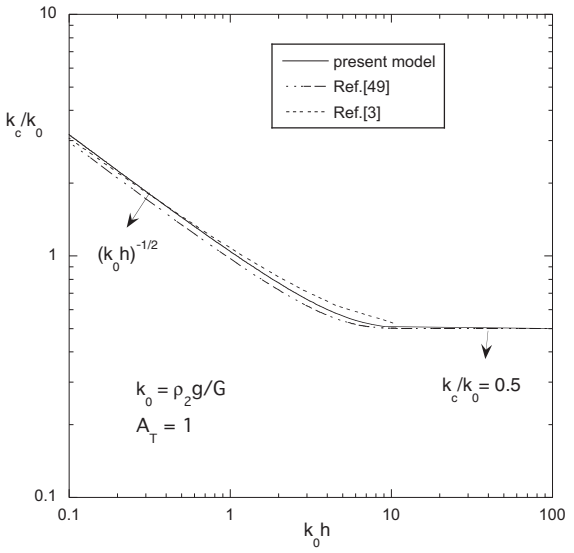

FIG. 3. Dimensionless cutoff wave number $\kappa_c = k_c/k_0$ as a function of the dimensionless slab thickness $a = k_0 h$ for $A_T = 1$. The solid line is the result of the present model, the dotted line is given in Refs. [3,4], and the dash-dotted line is obtained from the theory of Ref. [49].

We can get an analytical expression for κ_c by taking $\sigma = 0$ in Eq. (29):

$$\kappa_c \tanh \frac{a\kappa_c}{2} = \frac{A_T}{1 + A_T}. \tag{30}$$

For $a \gg 1$, the previous equation yields

$$\kappa_c = \frac{A_T}{1 + A_T}, \tag{31}$$

in agreement with the exact results obtained in Refs. [35,49,50]. In the other extreme, for $a \ll 1$, we get

$$\kappa_c = \sqrt{\frac{2A_T}{1 + A_T}\frac{1}{a}}, \tag{32}$$

which differs by a factor of $(3/4)^{1/4}$ with respect to the results of Refs. [3,4,49] for $A_T = 1$. Figure 3 shows a comparison of Eq. (30) for $A_T = 1$ with the exact results of Ref. [49] and with the approximate result of Refs. [3,4] obtained by extrapolating the results for a very thin layer to an arbitrary thickness.

It may be worth noting that κ_c increases for a thinner slab. That is, the stabilizing effect of the elasticity becomes less effective as the thickness of the slab is reduced. As we saw in Sec. II A, the thickness of the slab does not play any role in determining the growth rate for $A_T = 1$; instead, it has a stabilizing effect (growth rate reduction) for $A_T < 1$. Then, it may seem somewhat unexpected that thinner elastic slabs are less stable than the thicker ones. However, this result can be easily explained in the framework of the present model as a consequence of the fact that the stabilizing elastic forces arise from the effect of the total strain across the slab thickness and not from the local strains on the interfaces. In fact, at the limit of an infinitesimally thin slab, local forces on both surfaces would become practically equal, and the only effect would

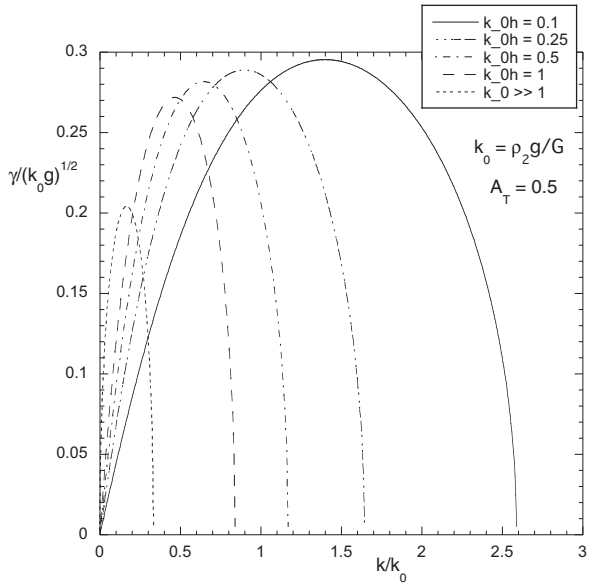

FIG. 4. Asymptotic dimensionless growth rate $\sigma = \gamma/\sqrt{k_0 g}$ as a function of the dimensionless wave number $\kappa = k/k_0$ for several values of $a = k_0 h$ and $A_T = 0.5$.

be a vertical translation of the slab, with no effective total restoring force acting on the slab ($S = 0$).

For $A_T < 1$, the stabilizing effect of thinner slabs shown in Eq. (13) becomes operative, and it will be in competition with the effect of the thickness on the elastic force. Such a competition can be seen in Fig. 4, where the growth rate is shown to be lower for the thinnest slabs at the longest wavelengths (smallest k) when the stabilizing effects of the elasticity are less important (as in the ideal case). Conversely, the growth rate becomes larger for the thinnest slabs at the shortest wavelengths (largest k) when the elastic stabilization is more effective.

Finally, we can see that the effect of the Atwood number is, as expected, to reduce the growth rate the smaller A_T is. This is shown in Fig. 5 for the fixed value of $a = 0.1$ [38].

B. Asymptotic feedthrough factor

We can describe the magnitude at which the perturbation is transmitted from the naturally unstable interface at $y = 0$ to the top interface at $y = -h$ by calculating the feedthrough factor $F = \xi_b/\xi$ in the asymptotic regime [52]:

$$F = \frac{\xi_b}{\xi} = \frac{\dot{\xi}_b}{\dot{\xi}}. \tag{33}$$

By using Eqs. (22) and (23) with S given by Eq. (25) and introducing the dimensionless magnitudes defined in Eq. (27), we get, after some straightforward algebra, the following expression:

$$F = \frac{e^{-a\kappa} + f e^{a\kappa}}{1+f} - 8\left[\frac{\kappa e^{-a\kappa}\sinh a\kappa}{(1+f)(\sigma^2+\kappa)}\right]^2 \times \left(\sigma^2 + \kappa \tanh\frac{a\kappa}{2}\right). \tag{34}$$

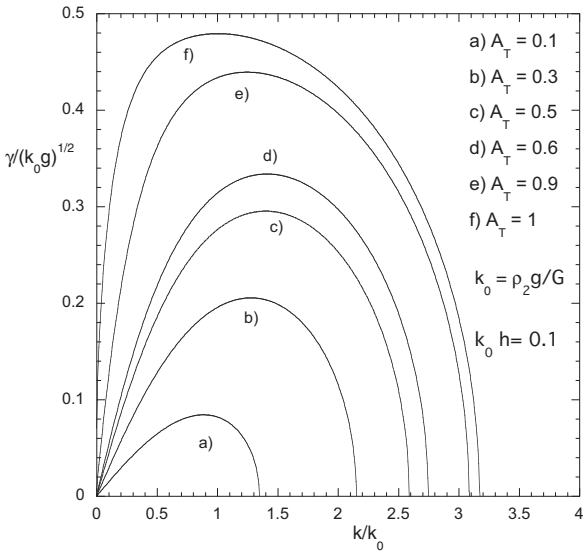

FIG. 5. Asymptotic dimensionless growth rate $\sigma = \gamma/\sqrt{k_0 g}$ as a function of the dimensionless wave number $\kappa = k/k_0$ for several values of A_T and $a = k_0 h = 0.1$.

It is not difficult to find the following limits of the previous equation:

$$F \to 1, \quad \kappa \to 0,$$
$$F \to -1, \quad \kappa \to \kappa_c. \tag{35}$$

We have represented Eq. (34) in Fig. 6 for $A_T = 1$ and for several values of $a = k_0 h$. As expected, the feedthrough factor is larger for the thinnest slabs, and at the limit $k \to 0$, it achieves the value $F = 1$. More interesting is the value of $F = -1$ for $\kappa = \kappa_c$, indicating that at such a limit both interfaces are oscillating at counterphase with the same amplitude, which could be expected for the respective extremes of a free oscillator. In fact, for larger values of κ the perturbation sees

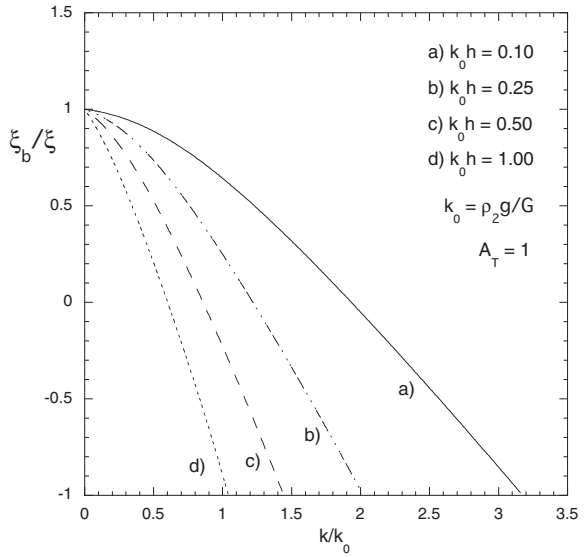

FIG. 6. Feedthrough factor $F = \xi_b/\xi$ as a function of the dimensionless wave number $\kappa = k/k_0$ for several values of $a = k_0 h$ and $A_T = 1$.

a relatively thicker slab, so that the feedthrough is reduced up to the point at which $\xi_b = 0$, and no perturbation is transmitted to the stable interface. A further increase of κ leads to an additional reduction of such an influence, and the restoring elastic force at $y = -h$ makes both surfaces oscillate at counterphase at $\kappa = \kappa_c$.

IV. CONCLUDING REMARKS

We have developed an analytical model for describing the linear RTI of a perfectly elastic solid slab that considers the effects of the slab finite thickness. By following previous works, the elastic forces are introduced as boundary conditions at the edges of the slab.

On the other hand, the effects of the finite thickness of the slab are taken into account by considering that, for a sufficiently thin slab, the transit time of the elastic waves across its thickness becomes shorter than the instability growth time, so that the restoring elastic force at the interfaces is determined by the total strain of the slab rather than by the local strains near the interfaces.

The results are in excellent agreement with the exact theory of Ref. [49] for $A_T = 1$ and reduce to the model of Ref. [35] for a very large thickness. The model provides a physical explanation for the seemingly unexpected loss of effectiveness of the elasticity in providing stabilization for the thinnest solid slabs. In fact, the thinner the slab is, the shorter the transit time is between the top and bottom interfaces, and the more uniform the strain is across the slab, thus reducing the total restoring force S on the interfaces. This effect is in competition with the growth rate reduction observed in an ideal medium slab for the smaller thicknesses.

In addition, it is not difficult to consider that the semi-infinite light medium is nonideal and/or that it contains a magnetic field, as done in Refs. [35,44–46] for two semi-infinite media.

The feedthrough factor F quantifying the magnitude of the transmission of the perturbation from the naturally unstable bottom interface to the top one is found to decrease with the slab thickness, and as expected, it is $|F| < 1$.

The model is seen to be a good candidate for being extended to include the effects of the finite thickness on the RTI in an elastic-plastic slab by considering the transition from the elastic to the plastic regime, in a manner similar to what was done in Ref. [42] for a semi-infinite solid.

ACKNOWLEDGMENTS

This work has been partially supported by the Ministerio de Economía y Competitividad of Spain (Grants No. ENE2013-45661-C2-1-P and No. ENE2016-75703-R) and by the BMBF of Germany.

APPENDIX A: THE IDEAL VELOCITY FIELD

Equations (2) and (3) are obtained by solving the linearized equations for momentum and mass conservation:

$$\rho\left[\frac{\partial \vec{v}}{\partial t} + (\vec{v}\cdot\vec{\nabla})\vec{v}\right] = -\vec{\nabla}p + \rho\vec{g}, \tag{A1}$$

$$\frac{\partial \rho}{\partial t} + (\vec{v}\cdot\vec{\nabla})\rho = -\rho\vec{\nabla}\cdot\vec{v}. \tag{A2}$$

Assuming that every magnitude φ ($\vec{v}$, p, and ρ) can be written as $\varphi = \varphi_0 + \delta\varphi$, with $\delta\varphi$ being the perturbation and φ_0 representing the unperturbed values, the equations for the perturbations are obtained:

$$\rho_0\frac{\partial(\delta v_x)}{\partial t} = -\frac{\partial(\delta p)}{\partial x}, \tag{A3}$$

$$\rho_0\frac{\partial(\delta v_y)}{\partial t} = -\frac{\partial(\delta p)}{\partial y}, \tag{A4}$$

$$\frac{\partial(\delta v_x)}{\partial x} = -\frac{\partial(\delta v_y)}{\partial y}, \tag{A5}$$

where we have taken $\vec{v}_0 = 0$ and $\vec{\nabla}\rho_0 = 0$ and we have considered incompressible perturbations ($\delta\rho = 0$). The solution of these equations is straightforward, and it reads [51,52]

$$\delta v_y = (C_+e^{ky} + C_-e^{-ky})e^{ikx} = -i\delta v_x, \tag{A6}$$

$$\delta p = -\frac{\rho_0}{k}(\dot{C}_+e^{ky} - \dot{C}_-e^{-ky})e^{ikx}. \tag{A7}$$

By taking $\rho_0 \equiv \rho_1$ for $y \geqslant 0$ and requiring that $\delta v_y \equiv \delta v_{1y} \to 0$ and $\delta p \equiv \delta p_1 \to 0$ when $y \to \infty$, it turns out $C_+ = 0$, and $C_- \equiv B_-$. Similarly, for $-h \leqslant y \leqslant 0$, we have $\rho_0 \equiv \rho_2$, $\delta v_y \equiv \delta v_{2y}$, $\delta p \equiv \delta p_2$, $C_\pm \equiv A_\pm$, and Eqs. (2) and (3) are obtained.

APPENDIX B: THE EXACT SOLUTION

In order to further check the goodness of the approximate model, we will outline here the derivation of the exact solution of the problem. The details will be presented elsewhere.

We start with the linearized equations for incompressible perturbations. For the heavy elastic medium ($y < 0$) we have

$$\frac{\partial(\delta v_{2i})}{\partial x_i} = 0, \tag{B1}$$

$$\rho_2\frac{\partial(\delta v_{2i})}{\partial t} = -\frac{\partial(\delta p_2)}{\delta x_i} + \frac{\partial S_{ik}}{\partial x_k}, \tag{B2}$$

$$\frac{\partial(S_{ik})}{\partial t} = 2GD_{ik}, \quad D_{ik} = \frac{1}{2}\left[\frac{\partial(\delta v_{2i})}{\partial x_k} + \frac{\partial(\delta v_{2k})}{\partial x_i}\right], \tag{B3}$$

where D_{ik} is the strain rate tensor. In order to get the velocity field for $y < 0$ we adopt the Helmholtz decomposition for which the velocity field can be expressed as the sum of a part $\delta\vec{v}_2^{\,\phi}$ given by the gradient of a scalar function ϕ_2 plus another part $\delta\vec{v}_2^{\,\psi}$ consisting of the curl of a solenoidal (zero divergence) vector $\psi_2\,\hat{e}_z$ [59,64,65]:

$$\delta\vec{v}_2 = \vec{\nabla}\phi_2 + \vec{\nabla}\times(\psi_2\,\hat{e}_z), \tag{B4}$$

where $\hat{e}_z$ is the unitary vector in the direction normal to the (x,y) plane, and by adopting the Bernoulli gauge [65], the potentials ϕ_2 and ψ_2 must satisfy the following equations:

$$\nabla^2\phi_2 = 0, \quad \gamma\psi_2 = \frac{G}{\gamma}\nabla^2\psi_2, \tag{B5}$$

where we have assumed that $\psi_2 \propto e^{\gamma t}$. By taking

$$\phi_2 \propto e^{(\gamma t + qy)}\sin kx, \quad \psi_2 \propto e^{(\gamma t + q'y)}\cos kx, \tag{B6}$$

the previous equations yield

$$q = \pm k, \quad q' = \pm\lambda, \quad \lambda = \sqrt{k^2 + \frac{\gamma^2\rho_2}{G}}. \tag{B7}$$

Then, the velocity field is given by the following equations [59,64,65]:

$$\delta v_{2y} = \frac{\partial\phi_2}{\partial y} - \frac{\partial\psi_2}{\partial x}, \quad \delta v_{2x} = \frac{\partial\phi_2}{\partial x} + \frac{\partial\psi_2}{\partial y}. \tag{B8}$$

It is convenient to take ϕ_2 and ψ_2 in the following form:

$$\phi_2 = \frac{a_2\cosh ky + b_2\cosh k(h+y)}{\sinh kh} e^{\gamma t}\sin kx, \tag{B9}$$

$$\psi_2 = \frac{a_2\sinh \lambda y + b_2\sinh \lambda(h+y)}{\sinh \lambda h} e^{\gamma t}\cos kx. \tag{B10}$$

On the other hand, for the light ideal fluid ($y > 0$) we have

$$\phi_1 = a_1 e^{-ky} e^{\gamma t}\sin kx, \quad \delta v_{1y} = \frac{\partial\phi_1}{\partial y}, \quad \delta v_{1x} = \frac{\partial\phi_1}{\partial x}. \tag{B11}$$

Since the tangential stress S_{xy} must be equal to zero at $y = 0$ and $y = -h$, we get

$$d_2 = -\frac{2k^2}{\lambda^2 + k^2} b_2, \quad c_2 = -\frac{2k^2}{\lambda^2 + k^2} a_2. \tag{B12}$$

In addition, the continuity of the normal stress $-\delta p + S_{yy} = -\delta p + (G/\gamma)\partial(\delta v_y)/\partial y$ at $y = -h$ and $y = 0$, respectively, leads to the following dynamical conditions on the moving interfaces:

$$\frac{\partial\phi_2(-h)}{\partial t} + S_{yy}(-h) + g\xi_b = 0, \tag{B13}$$

$$\frac{\partial\phi_2(0)}{\partial t} + S_{yy}(0) + g\xi = \frac{\rho_1}{\rho_2}\left[\frac{\partial\phi_1(0)}{\partial t} + g\xi\right], \tag{B14}$$

where the continuity of the vertical velocity at $y = 0$ has been used ($-a_1 = b_2 + d_2$). Equations (B12) to (B14) yield the following relationships from which the growth rate γ can be obtained:

$$a_2\left(C - \frac{\rho_2 kg}{G}\right) + b_2 A = 0, \tag{B15}$$

$$a_2 A + b_2\left[C + \left(1 - \frac{\rho_1}{\rho_2}\right)\frac{\rho_2 kg}{G} - \frac{\gamma^2\rho_1}{G}\right] = 0, \tag{B16}$$

where C and A are defined as follows [49]:

$$C = \frac{(\lambda^2 + k^2)^2\cosh kh\sinh \lambda h - 4k^3\lambda\cosh \lambda h\sinh kh}{(\lambda^2 - k^2)\sinh kh\sinh \lambda h}, \tag{B17}$$

$$A = \frac{(\lambda^2 + k^2)^2\sinh \lambda h - 4k^3\lambda\sinh kh}{(\lambda^2 - k^2)\sinh kh\sinh \lambda h}. \tag{B18}$$

From the previous equations we can get the cutoff wave number k_c by taking $\gamma = 0$. In such a limit we have

$$Ch^2 = \frac{x^2(2x - \sinh 2x)}{(\sinh x)^2}, \tag{B19}$$

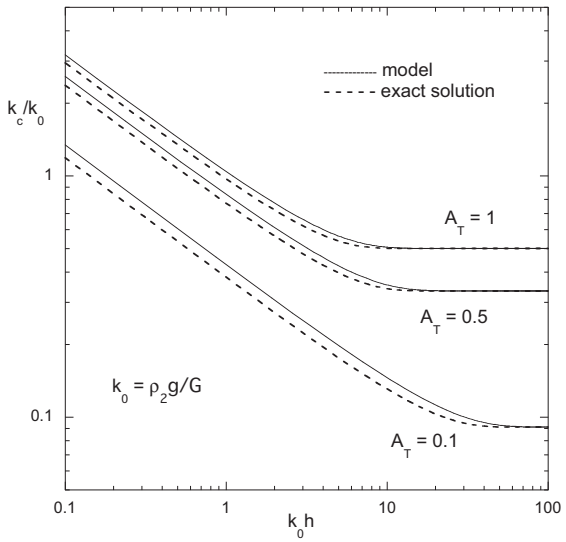

FIG. 7. Dimensionless cutoff wave number $\kappa_c = k_c/k_0$ as a function of the dimensionless slab thickness $a = k_0 h$ for several values of A_T. Solid lines are given by Eq. (30), and dotted lines are the results of the exact theory outlined in Appendix B.

$$Ah^2 = \frac{2x^2(x\cosh x - \sinh 2x)}{(\sinh x)^2}, \tag{B20}$$

where $x = k_c h = a\kappa_c$. Then, from Eqs. (B15) and (B16) we obtain the following quadratic equation:

$$a^2 + aF_1(x) - F_2(x) = 0, \tag{B21}$$

$$F_1(x) = \frac{1 - A_T}{2A_T}\frac{Ch^2}{x}, \tag{B22}$$

$$F_2(x) = \frac{2(1 + A_T)}{A_T} x^1\left[1 - \left(\frac{x}{\sinh x}\right)^2\right]. \tag{B23}$$

Equations (B21) to (B23) give κ_c as a function of $a = k_0 h$ with A_T as a parameter. In Fig. 7 we show the solutions for $A_T = 0.1$, 0.5, and 1 (dotted lines). In the same figure we also illustrate the approximate calculations by means of Eq. (30) (solid lines), which are seen to be in excellent agreement with the exact results for any value of A_T. Equation (30) gives the exact cutoff wave number κ_c for $a \gg 1$, and it approximates the exact value within an error of around 10% for $a \ll 1$. In this latter limit Eq. (B21) yields an analytical expression:

$$\frac{1}{a^{1/2}\kappa_c} = \sqrt{\frac{1 - A_T}{3A_T} + \sqrt{\left(\frac{1 - A_T}{3A_T}\right)^2 + \frac{2(1 + A_T)}{3A_T}}}. \tag{B24}$$

It can easily be checked that the function of A_T on the right-hand side of the previous equation differs by around 10% from the corresponding factor in Eq. (32), for which it turns out to be an excellent approximation of the exact result.

The good results of the model based on the irrotational velocity field can be explained by the previous analysis. In fact, from Eq. (B7) we can see that when $k^2 \gg \gamma^2\rho_2/G$, the rotational part $\delta\vec{v}_2^{\,\psi}$ of the velocity field becomes indistinguishable from the irrotational part, although it can be a considerable

part of the total velocity field $\delta\vec{v}_2$, and therefore, neglecting the vorticity would not have a significant effect on the instability growth rate.

The opposite case, when $k^2 \ll \gamma^2\rho_2/G$, corresponds to the situation in which the shear modulus G becomes relatively small, and although the rotational component of the velocity field is well differentiated from the irrotational part, it becomes a small part of the total velocity field. This latter case is equivalent to the low Reynolds number flows in viscous fluids, and it is well known they correspond to the physical realization of an ideal flow [66].

Then, the maximum departure from the exact results should be expected for the wave numbers $k \sim \sqrt{\gamma^2\rho_2/G}$ ($\kappa \sim \sigma$). That is, even in the worst case the velocity field is not extremely different from the irrotational part, and therefore, the results obtained by neglecting the rotational part must always be reasonably good. An example of a situation with $\kappa \sim \sigma$ appears in the neighborhood of the maximum growth rate for $k_0 h \gg 1$ (Fig. 2), where a maximum error of 18% is found [35]. In other cases, the maximum growth rate shifts toward larger values of κ, and it becomes $\sigma < \kappa$, thus improving the accuracy of the irrotational approximation.

[1] J. F. Barnes, P. J. Blewet, R. G. McQueen, K. A. Meyer, and D. Venable, J. Appl. Phys. **45**, 727 (1974).

[2] J. F. Barnes, D. H. Janney, R. K. London, K. A. Meyer, and D. H. Sharp, J. Appl. Phys. **51**, 4678 (1980).

[3] S. M. Bakhrakh, O. B. Drennov, N. P. Kovalev, A. I. Lebedev, E. E. Meshkov, A. L. Mikhailov, N. V. Neumerzhitsky, P. N. Nizovtsev, V. A. Rayevsky, G. P. Simonov, V. P. Solovyev, and I. G. Zhidov, Lawrence Livermore National Laboratory, Report No. UCRL-CR-126710, 1997 (unpublished), https://www.osti.gov/scitech/servlets/purl/515973

[4] A. I. Lebedev, P. N. Nisovtsev, and V. A. Rayevsky, in *Proceedings of the 4th International Workshop on the Physics of Compressible Turbulent Mixing (IWPCTM)*, 29 March–1 April 1993, Cambridge, England (Cambridge University Press, New York, 1993), p. 81.

[5] G. Dimonte, R. Gore, and M. Schneider, Phys. Rev. Lett. **80**, 1212 (1998).

[6] D. H. Kalantar, B. A. Remington, J. D. Colvin, K. O. Mikaelian, S. V. Weber, L. G. Wiley, J. S. Wark, A. Loveridge, A. M. Allen, A. A. Hauer, and M. A. Meyers, Phys. Plasmas **7**, 1999 (2000).

[7] J. D. Colvin, M. Legrand, B. A. Remington, G. Shurtz, and S. V. Weber, J. Appl. Phys. **93**, 5287 (2003).

[8] B. A. Remington, P. Allen, E. M. Bringa, J. Hawreliak, D. Ho, K. T. Lorenz, H. Lorenzana, J. M. McNaney, M. A. Meyers, S. W. Pollaine, K. Rosolankova, B. Sadik, M. S. Schneider, D. Swift, J. Wark, and B. Yaakobi, Mater. Sci. Technol. **22**, 474 (2006).

[9] K. O. Mikaelian, Phys. Plasmas **17**, 092701 (2010).

[10] H.-S. Park, K. T. Lorenz, R. M. Cavallo, S. M. Pollaine, S. T. Prisbrey, R. E. Rudd, R. C. Becker, J. V. Bernier, and B. A. Remington, Phys. Rev. Lett. **104**, 135504 (2010).

[11] N. A. Tahir, D. H. H. Hoffmann, A. Kozyreva, A. Tauschwitz, A. Shutov, J. A. Maruhn, P. Spiller, U. Neuner, J. Jacoby, M. Roth, R. Bock, H. Juranik, and R. Redmer, Phys. Rev. E **63**, 016402 (2000).

[12] A. R. Piriz, Phys. Fluids **31**, 658 (1988).

[13] A. R. Piriz, R. F. Portugues, N. A. Tahir, and D. H. H. Hoffmann, Phys. Rev. E **66**, 056403 (2002).

[14] A. R. Piriz, R. F. Portugues, N. A. Tahir, and D. H. H. Hoffmann, Laser Part. Beams **20**, 427 (2002).

[15] N. A. Tahir, H. Juranek, A. Shutov, R. Redmer, A. R. Piriz, M. Temporal, D. Varentsov, S. Udrea, D. H. H. Hoffmann, C. Deutsch, I. Lomonosov, and V. E. Fortov, Phys. Rev. B **67**, 184101 (2003).

[16] N. A. Tahir, P. Spiller, A Shutov, I. V. Lomonosov, V. Gryaznov, A. R. Piriz, G. Wouchuk, C. Deutsch, F. Fortov, D. H. H. Hoffmann, and R. Schmidt, Nucl. Instrum. Methods Phys. Res., Sect. A **577**, 238 (2007).

[17] M. Temporal, A. R. Piriz, N. Grandjouan, N. A. Tahir, and D. H. H. Hoffmann, Laser Part. Beams **21**, 609 (2003).

[18] N. A. Tahir, P. Spiller, S. Udrea, O. D. Cortazar, C. Deutsch, V. E. Fortov, V. Gryaznov, D. H. H. Hoffmann, I. V. Lomonosov, P. Ni, A. R. Piriz, A. Shutov, M. Temporal, and D. Varentsov, Nucl. Instrum. Methods Phys. Res., Sect. B **245**, 85 (2006).

[19] N. A. Tahir, V. V. Kim, A. V. Matvechev, A. V. Ostrik, A. V. Shutov, I. V. Lomonosov, A. R. Piriz, J. J. López Cela, and D. H. H. Hoffmann, Laser Part. Beams **26**, 273 (2008).

[20] N. A. Tahir, T. Stoehlker, A. Shutov, I. V. Lomonosov, V. E. Fortov, M. French, N. Nettelmann, R. Redmer, A. R. Piriz, C. Deutsch, Y. Zhao, P. Zhang, H. Xu, G. Xiao, and W. Zhan, New J. Phys. **12**, 073022 (2010).

[21] A. R. Piriz, N. A. Tahir, D. H. H. Hoffmann, and M. Temporal, Phys. Rev. E **67**, 017501 (2003).

[22] A. R. Piriz, M. Temporal, J. J. López Cela, N. A. Tahir, and D. H. H. Hoffmann, Plasma Phys. Controlled Fusion **45**, 1733 (2003).

[23] R. E. Reinovsky, W. E. Anderson, W. L. Atchison, C. E. Ekdahl, R. J. Faehl, I. R. Lindemuth, D. V. Morgan, M. Murillo, J. L. Stokes, and J. S. Shlachter, IEEE Trans. Plasma Sci. **30**, 1764 (2002).

[24] C. A. Hall, J. R. Asay, M. D. Knudsen, W. A. Stygan, R. B. Spielman, T. D. Pointon, D. B. Reisman, A. Toor, and R. C. Cauble, Rev. Sci. Instrum. **72**, 3587 (2001).

[25] S. A. Slutz, M. C. Herrmann, R. A. Vesey, A. B. Sefkow, D. B. Sinars, D. C. Rovang, K. J. Peterson, and M. E. Cuneo, Phys. Plasmas **17**, 056303 (2010).

[26] D. B. Sinars, S. A. Slutz, M. C. Herrmann, R. D. McBride, M. E. Cuneo, K. J. Peterson, R. A. Vesey, C. Nakhleh, B. E. Blue, K. Killebrew, D. Schroen, K. Tomlinson, A. D. Edens, M. R. López, I. C. Smith, J. Shores, V. Bigman, G. R. Bennett, B. W. Atherton, M. Savage, W. A. Stygar, G. T. Leifeste, and J. L. Porter, Phys. Rev. Lett. **105**, 185001 (2010).

[27] D. B. Sinars, S. A. Slutz, M. C. Herrmann, R. D. McBride, M. E. Cuneo, C. A. Jennings, J. P. Chittenden, A. L. Velikovich, K. J. Peterson, R. A. Vesey, C. Nakhleh, E. M. Waisman, B. E. Blue, K. Killebrew, D. Schroen, K. Tomlinson, A. D. Edens, M. R. López, I. C. Smith, J. Shores, V. Bigman, G. R. Bennett, B. W. Atherton, M. Savage, W. A. Stygar, G. T. Leifeste, and J. L. Porter, Phys. Plasmas **18**, 056301 (2011).

[28] R. D. McBride, M. R. Martin, R. W. Lemke, J. B. Greenly, C. A. Jennings, D. C. Rovang, D. B. Sinars, M. E. Cuneo, M. C. Herrmann, S. A. Slutz, C. W. Nakhleh, D. D. Ryutov, J.-P. Davis, D. G. Flicker, B. E. Blue, K. Tomlinson, D. Schroen, R. M. Stamm, G. E. Smith, J. K. Moore, T. J. Rogers, G. K. Robertson, R. J. Kamm, I. C. Smith, M. Savage, W. A. Stygar, G. A. Rochau, M. Jones, M. R. López, J. L. Porter, and M. K. Matzen, Phys. Plasmas **20**, 056309 (2013).
[29] A. Bret, A. R. Piriz, and N. Tahir, Phys. Rev. E **85**, 036402 (2012).
[30] A. R. Piriz, J. J. López Cela, N. A. Tahir, and D. H. H. Hoffmann, Phys. Rev. E **78**, 056401 (2008).
[31] G. Dimonte, G. Terrones, F. J. Cherne, T. C. Germann, V. Dupont, K. Kadau, W. T. Buttler, D. M. Oro, C. Morris, and D. L. Preston, Phys. Rev. Lett. **107**, 264502 (2011).
[32] W. T. Buttler, D. M. Oro, D. L. Preston, K. O. Mikaelian, F. J. Cherne, R. S. Hixson, F. G. Mariam, C. Morris, J. B. Stone, G. Terrones, and D. Tupa, J. Fluid. Mech. **703**, 60 (2012).
[33] G. Dimonte, G. Terrones, F. J. Cherne, and P. Ramaprabhu, J. Appl. Phys. **113**, 024905 (2013).
[34] M. B. Prime, D. E. Vaughan, D. L. Preston, W. T. Buttler, S. R. Chen, D. M. Oro, and C. Pack, J. Phys. Conf. Ser. **500**, 112051 (2014).
[35] A. R. Piriz, J. J. López Cela, O. D. Cortazar, N. A. Tahir, and D. H. H. Hoffmann, Phys. Rev. E **72**, 056313 (2005).
[36] A. R. Piriz, O. D. Cortazar, J. J. López Cela, and N. A. Tahir, Am. J. Phys. **74**, 1095 (2006).
[37] A. R. Piriz, J. J. López Cela, N. A. Tahir, and D. H. H. Hoffmann, Phys. Rev. E **74**, 037301 (2006).
[38] A. R. Piriz, J. J. López Cela, M. C. Serna Moreno, N. A. Tahir, and D. H. H. Hoffmann, Laser Part. Beams **24**, 275 (2006).
[39] J. J. López Cela, A. R. Piriz, M. C. Serna Moreno, and N. A. Tahir, Laser Part. Beams **24**, 427 (2006).
[40] A. R. Piriz, J. J. López Cela, and N. A. Tahir, Nucl. Instrum. Methods Phys. Res., Sect. A **606**, 139 (2009).
[41] A. R. Piriz, J. J. López Cela, and N. A. Tahir, J. Appl. Phys. **105**, 116101 (2009).
[42] A. R. Piriz, J. J. López Cela, and N. A. Tahir, Phys. Rev. E **80**, 046305 (2009).
[43] A. R. Piriz, J. J. López Cela, and N. A. Tahir, Phys. Rev. Lett. **105**, 179601 (2010).
[44] A. R. Piriz, Y. B. Sun, and N. A. Tahir, Phys. Rev. E **88**, 023026 (2013).
[45] A. R. Piriz, Y. B. Sun, and N. A. Tahir, Phys. Rev. E **89**, 063022 (2014).
[46] Y. B. Sun and A. R. Piriz, Phys. Plasmas **21**, 072708 (2014).
[47] A. R. Piriz, Y. B. Sun, and N. A. Tahir, Eur. J. Phys. **38**, 015003 (2017).
[48] A. R. Piriz, Y. B. Sun, and N. A. Tahir, Phys. Rev. E **91**, 033007 (2015).
[49] B. J. Plohr and D. H. Sharp, Z. Angew. Math. Mech. **49**, 786 (1998).
[50] G. Terrones, Phys. Rev. E **71**, 036306 (2005).
[51] G. I. Taylor, Proc. R. Soc. London, Ser. A **201**, 192 (1950).
[52] V. N. Goncharov, P. McKenty, S. Skupsky, R. Betti, R. L. McCrory, and C. Cherfils-Clérouin, Phys. Plasmas **7**, 5118 (2000).
[53] K. O. Mikaelian, Phys. Rev. A **26**, 2140 (1982).
[54] K. O. Mikaelian, Phys. Rev. A **28**, 1637 (1983).
[55] K. O. Mikaelian, Phys. Rev. A **42**, 7211 (1990).
[56] Y. Y. Lau, J. C. Zier, I. M. Rittersdorf, M. R. Weis, and R. M. Gilgenbach, Phys. Rev. E **83**, 066405 (2011).
[57] M. R. Weis, P. Zhang, Y. Y. Lau, I. M. Rittersdorf, J. C. Zier, R. M. Gilgenbach, M. H. Hess, and K. J. Peterson, Phys. Plasmas **21**, 122708 (2014).
[58] M. S. Plesset and C. G. Whipple, Phys. Fluids **17**, 1 (1974).
[59] W. Harrison, Proc. London Math. Soc. **s2-6**, 396 (1908).
[60] H. Ramberg, Phys. Earth Planet. Inter. **1**, 427 (1968).
[61] W. S. D. Wilcock and J. A. Whitehead, J. Geophys. Res. **96**, 12193 (1991).
[62] S. Parhi and G. Nath, Int. J. Eng. Sci. **29**, 1439 (1991).
[63] K. O. Mikaelian, Phys. Rev. E **54**, 3676 (1996).
[64] H. Lamb, *Hydrodynamics* (Dover, New York, 1945).
[65] R. Menikoff, R. C. Mjolness, D. H. Sharp, C. Zemach, and B. J. Doyle, Phys. Fluids **21**, 1674 (1978).
[66] D. Joseph, T. Funada, and J. Wang, *Potential Flows of Viscous and Viscoelastic Fluids* (Cambridge University Press, New York, 2007).